Silicon (2022) 14:3419–3427
https://doi.org/10.1007/s12633-021-01125-0

ORIGINAL PAPER

Research on the Effects of Yttrium on Bismuth Titanate Borosilicate Glass System

K.H. Mahmoud [1] · A.SA. Alsubaie [1] · E. A. Abdel Wahab [2] · Farid M. Abdel-Rahim [2] · Kh. S. Shaaban [3]

Received: 27 February 2021 / Accepted: 19 April 2021 / Published online: 25 April 2021

Abstract

Glasses with the chemical composition of $52B_2O_3 - 12SiO_2–26Bi_2O_3 - (10-x)TiO_2$ - xY_2O_3, :$(0 \le x \le 10)$ prepared using the melt-quench method. The goal of this study is to investigate the structural, mechanical, and radiation shielding characteristics of these samples. XRD analysis has explored the nature of the glass system. Molar volume obtained reduced while the density denotes increased in the present system. As the molar volume decrease inter-ionic distance, polaron radius, inter-nuclear distance, and Y-Y separation of the investigated glasses decreased. The mechanical characteristics depend on the glass structure of the current glasses sample. Ultrasonic velocities and elastic moduli (experimental and theoretical) for these glasses obtained they were observed to get enhanced. The radiation shielding efficiency was investigated by Phy-X/PSD software. The mass attenuation coefficient, mean free path, half-value layer, tenth value layer, and effective atomic number of glasses have been designed to simulate gamma photon energies between 0.015 and 15 MeV.

Keywords Glasses · Y_2O_3 · Elastic modulus · Radiation shielding

1 Introduction

Due to the importance of glass materials containing many transition metal ions (TMI) for many applications, these glasses have existed intersected over the past few years. In specific, the glass based on B_2O_3 and SiO_2 has become common among a wide variety of glass systems, keeping in mind its glass status, transparency, and a variety of physical and chemical properties. The B element can transform its coordination number between 3 and 4 with oxygen supplying by modification of metal cations [1–5]. Due to their unique properties such as hardness, transparency, UV-transmission ability, and corrosion resistance, SiO_2-B_2O_3 glasses were investigated for many years. B_2O_3- SiO_2 glass modified with Bi_2O_3 is characterized by its excellent optical, mechanical, radiation, and electrical properties [5–12].

The physical characteristics of the glass change based on its formulation and can be linked with the network structures and interatomic forces. Glasses with more bridging oxygen (BOs) have a more compact glass framework and high elastic moduli. Introducing Y_2O_3 to SiO_2 - B_2O_3 glasses improve chemical stability durability, a vast compositional variety of glass forming, and increased transmission with promising properties reported. The presence of trivalent oxide like Y_2O_3 in borosilicate glass exhibits dual nature as former or intermediate in the glass network. These glasses obtained noticed to withstand atmospheric moisture and are accept a good quantity of doping transition metal (TM) or rare-earth (REs) [13, 14].

Glasses doped intermediate oxides such as TiO_2 and Y_2O_3 have specific mechanical and optical characteristics such as hardness, elastic moduli, and higher refractive index [15–18]. It is also significant to observe that the inclusion of Y_2O_3 improves the capability of UV transmission, enhances thermal stability and chemical durability. The emergence of Y_2O_3 into the glass network improved the glass's mechanical, thermal, and shielding characteristics [19]. Because of the good conductivity of these glasses in ionic terms, it is probable to use them in UV optics, solid-state batteries, and radiation

✉ Kh. S. Shaaban
khamies1078@yahoo.com

1 Department of Physics, College of Khurma University College, Taif University, P.O. Box11099, Taif 21944, Saudi Arabia

2 Physics Department, Faculty of Science, Al-Azhar University, P O. 71524, Assiut, Egypt

3 Chemistry Department, Faculty of Science, Al-Azhar University, P.O. 71524, Assiut, Egypt

Table 1 Chemical composition of prepared glasses (mol. %)

Sample name	B_2O_3 mol.%	SiO_4	Bi_2O_3	TiO_2	Y_2O_3
G1	52	12	26	10	0
G2	52	12	26	8	2
G3	52	12	26	4	6
G4	52	12	26	2	8
G5	52	12	26	0	10

protection. These glasses possess lower photon energy and a greater refractive index than other glasses. The significant development of bismuth yttrium titanate borosilicate glasses is very important scientifically and technologically. The best candidate for photon shielding applications is $52B_2O_3 - 12SiO_2 - 26Bi_2O3$- (10-$x$)$TiO_2$- xY_2O_3, :($0 \leq x \leq 10$) a glass system. Acquiring the physical and mechanical values of these glasses can aid in the development of a variety of equipment and innovations, such as batteries, and gamma ray protection. The recent glasses displayed excellent properties for use in mechanical and radiation shielding applications. The creativity of this research paper is reflected in the structural, mechanical, and radiation shielding characteristics of $B_2O_3 - SiO_2 - Bi_2O_3$-TiO_2 glass undoped and doped with Y^{+3} ions.

2 Methodology

Five glass samples in Table 1 with the nominal compositions $52B_2O_3 - 12SiO_2 - 26Bi_2O_3$- (10-$x$)$TiO_2$- xY_2O_3, :($0 \leq x \leq 10$) prepared using the solid-state conventional method. By melting together specific weights of B_2O_3 in the form of H_3BO_3 (Merck), SiO_2 (Aldrich), Bi_2O_3 (Merck), TiO_2 (Merck), and Y_2O_3 (Merck) in an open porcelain crucible. H_3BO_3 converted into B_2O_3 after the H_2O evaporation

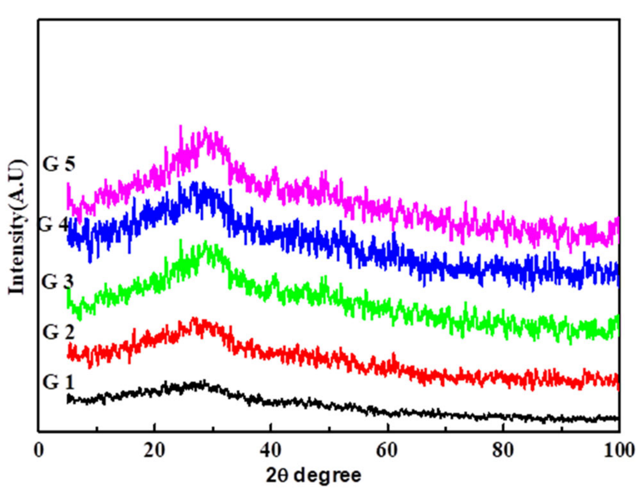

Fig. 1 XRD of the studied glasses

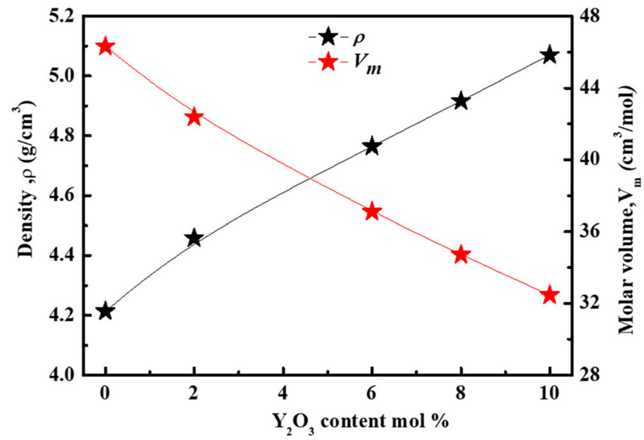

Fig. 2 Density and molar volume of the prepared samples versus Y_2O_3 concentration in mol %

process throughout the melting in porcelain crucibles. Thus, it is possible to estimate the required amount of oxide to match the chemical formula used by knowing the molecular weight of H_3BO_3, and B_2O_3. The porcelain crucible with the blend was kept at 650 °C for 45 min to decrease the tendency to volatilize. The furnace temperature programmed to rise to the melting temperature at 1150 °C and kept for 50 min. The melting glass was cast in a clean stainless-steel mold. After that, glass samples annealed at 400 °C to remove the internal stresses.

To verify the status of fabricated glasses, the Philips X-ray diffractometer (model PW/1710) was used. The densities of glasses were quantified by the Archimedes method. $\rho = \rho_0\left(\frac{M}{M-M_1}\right)$ where M and M_1 are the weights of samples in air and fluid, the glass density is ρ and the density of toluene is ρ_0 (0.865 g.cm^{-3}) with error ± 0.001 g.cm^{-3}. Using a pulse-echo method, the ultrasonic velocities estimation characterized (Echograph model 1085). The molar volume can evaluate as $V_m = \frac{M}{\rho}$ where M the molar weight of the glass. Besides the density, velocities are used to evaluate elastic

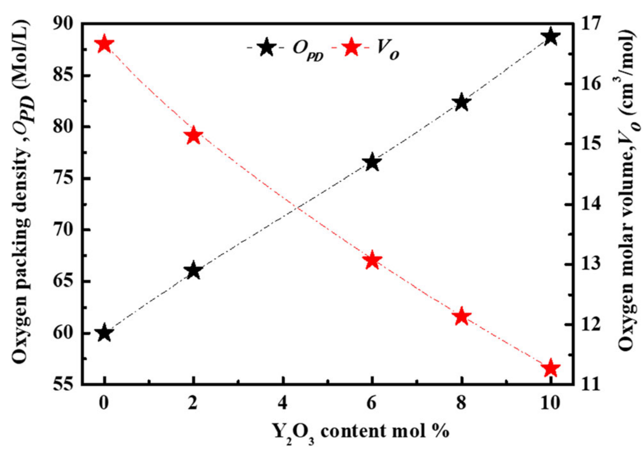

Fig. 3 Oxygen packing density and oxygen molar volume of the investigated glasses versus content of Y_2O_3 mol.%

Table 2 Various physical parameters of the studied glasses

Samples	G 1	G 2	G 3	G 4	G 5
Ion conc. (Y_i) (10^{21} ions/cm^3)	–	0.854	2.93	4.17	5.58
Inter ionic Distance R_i (Å)	–	10.71	7.11	6.32	5.73
Inter-nuclear distance, ri (Å)	–	12.4	8.24	7.33	6.66
Polaron radius, r_p (Å)	–	3.55	2.37	2.11	1.91
Y-Y separation(d_{Y-Y}), nm	0.61	0.59	0.55	0.54	0.52
Average coordination number (m)	3.94	3.98	4.06	4.1	4.14
Number of bonds per unit volume n_b (10^{28} m^{-3})	5.12	5.65	6.59	7.1	7.68
Bond-stretching constraints, N_{bs}	1.97	1.99	2.03	2.05	2.07
Bond-bending constraints, N_{bb}	2.44	2.48	2.56	2.6	2.64
Total number of constraints, N_{con}	4.41	4.47	4.59	4.65	4.71
The floppy modes, M_f	1.28	1.32	1.38	1.42	1.45
The cross-linking density, D_{CL}	2.41	2.47	2.59	2.65	2.71
Effective coordination number CN_{eff}	4.764	4.788	4.836	4.86	4.884

moduli. longitudinal waves $L=\rho v_l^2$, transverse waves $G=\rho v_t^2$, Young's modulus $Y=(1+\sigma)2G$, bulk modulus $K=L-\left(\frac{4}{3}\right)G$ The elastic moduli of the samples can be evaluated using the exemplary [20–23] based on packing density $Vi=\left(\frac{3\pi}{4}\right)N_A\,(m\mathrm{R}^3+n\,\mathrm{R}_\mathrm{O}^3)\,m^3.mol^{-1}$, and dissociation energy $Gi=\left(\frac{1}{V_m}\right)\sum_i GiXi$, the metallic and oxygen Pauling ionic radii are R_m and R_O. Longitudinal waves $L=K+\left(\frac{4}{3}\right)G$, transverse waves $G=30*\left(\frac{V_i^2G_i}{V_i}\right)$ Young's modulus $Y=8.36V_iG_i$, bulk modulus $K=10V_i^2G_i$. Poisson's ratio $\sigma=\frac{1}{2}-\left(\frac{1}{7.2*Vi}\right)$. Acoustic Impedance; $Z=v_L\rho$. Micro Hardness; $H=\frac{(1-2\sigma)Y}{6(1+\sigma)}$. Debye Temperature: $\theta_D=\frac{h}{k}\left(\frac{9N_A}{4\pi\,V_m}\right)^{\frac{1}{3}}M_s$, Where h and k are the constants of Planck and Boltzmann and N_A is the number of Avogadro [23, 24]. Average velocities $M_s=\frac{1}{3}\left(\frac{\frac{2}{v_T^3}}{\frac{1}{v_l^3}}\right)^{\frac{1}{3}}$, Thermal coefficient of expansion $\alpha_{P=23.2\ (v_L-0.57457)}$, the oxygen molar volume $V_o=\left(\frac{M}{\rho}\right)\left(\frac{1}{\sum xini}\right)$, Oxygen Packing Density $OPD=\left(\frac{1000\ C}{Vm}\right)\left(\frac{Mol}{L}\right)$.

In this article, radiation parameters have computed using Phy-X/PSD software [19], and these parameters calculated using the following equations: Beer-Lambert law $\mu=-\frac{ln\frac{I}{I_o}}{x}$,. Where μ the linear attenuation coefficient (cm^{-1}) I_0 and I respectively, the coefficient of mass attenuation samples $\left(\mu/\rho\right)=\sum_i x_i\left(\mu/\rho\right)_i$. Effective atomic number $Z_{eff}=\frac{\sum_i f_iA_i\left(\mu/\rho\right)_i}{\sum_j f_j\frac{A_j}{Z_j}\left(\mu/\rho\right)_j}$. Half and tenth value layer (HVL), and (TVL): $HVL=\frac{0.693}{LAC}$, $TVL=\frac{2.3}{LAC}$. The mean free path (MFP) was predictable as $MEP=\left(\frac{1}{\mu}\right)$.

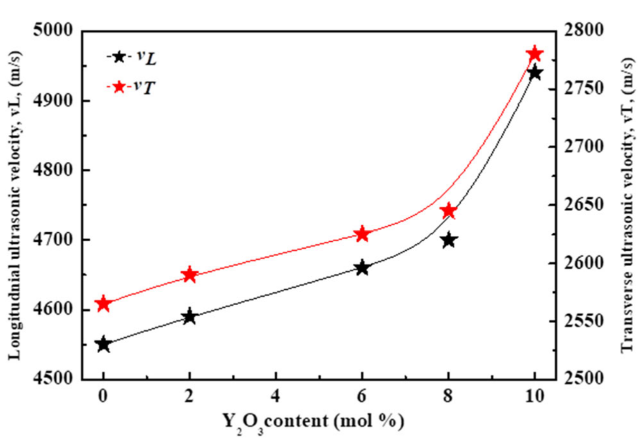

Fig. 4 Dependence of the longitudinal and shear ultrasonic velocities v_L and v_T of the investigated glasses with Y_2O_3 concentration by mol. %

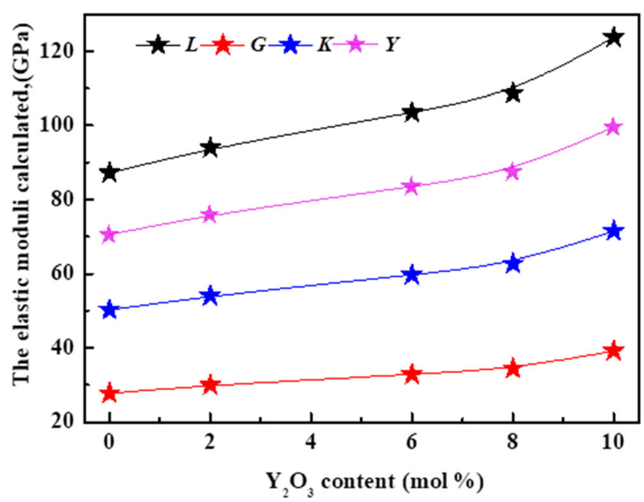

Fig. 5 Elastic moduli calculated of the studied glasses with Y_2O_3 content by mol. %

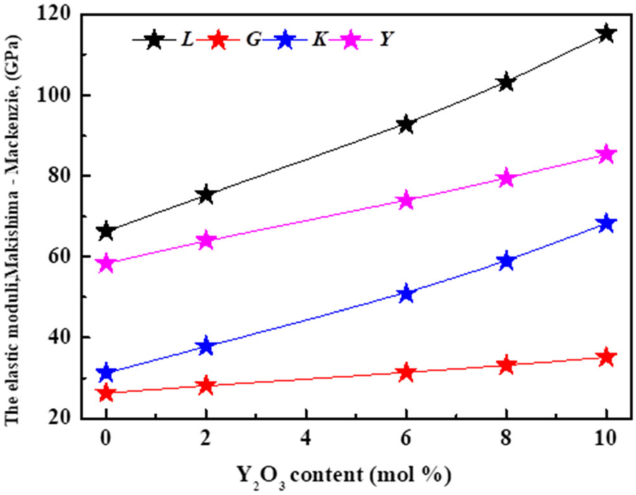

Fig. 6 Elastic moduli theoretically of the studied glasses with Y_2O_3 content by mol. %, according to Makishima – Mackenzie Model

3 Results and Discussion

3.1 XRD

The XRD characteristic of the glass with a wide hollow band at 2θ° between (20° - 30°) demonstrated in Fig. 1, which signifies the amorphous status of the glass. The width of the small mound differs from one sample to another but is not no indications of the crystalline phases have displayed in all the glasses. The two humps around (~25) 2θ° values concerning Y_2O_3 concentration can be related to the decrease in the bond length and the higher coordination number with oxygen.

3.2 Physical Studies

Different factors, such as chemical constituents and internal structure have affected the density of $52B_2O_3$ – $12SiO_2$ – $26Bi_2O_3$-$(10-x)$ TiO_2- xY_2O_3, $where\ x:(0\leq x\leq 10)$ glass system. Its values are in the range 4.213–5.07 g/cm^3 for different glass compositions and it follows a linear trend. The

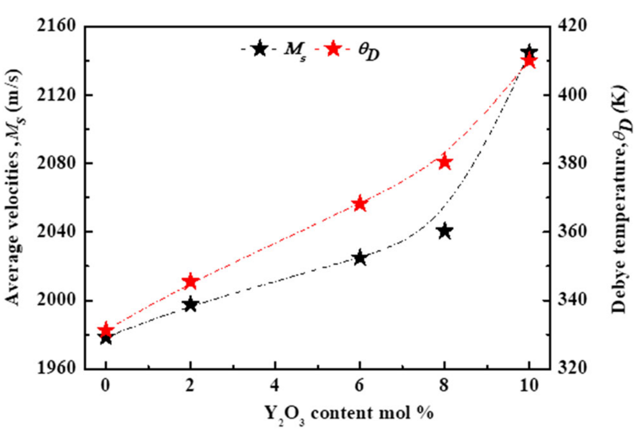

Fig. 7 Debye temperature and average velocities of the studied glasses with Y_2O_3 concentration by mol. %

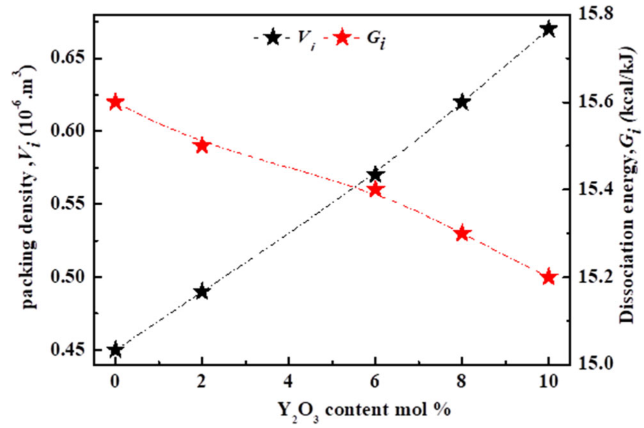

Fig. 8 Values of packing density (Vi), dissociation energy (Gi), of glass system doped and undoped Y_2O_3 oxide by mol. %

density of the glass under investigation increases with the increment in the content of Y_2O_3. This observation because of the high Y_2O_3 density (5.03 g/cm^3) relative to TiO_2 (4.23 g/cm^3) and the high Y_2O_3 atomic mass (225.81) relative to TiO_2 (79.866). The emergence of Y_2O_3 in a glass matrix enhances the structural network by raising the oxygen level, resulting in the transformation of BO_3 into BO_4 units, and may also another reason lead to an increase in glass density. In the science of glass, the molar volume also plays an important role. The reduction in molar volume could be related to the formation of bridging oxygens that reduce the voids within the configuration. The density and molar volume of prepared glasses are exemplified in Fig. 2 [20–22].

OPD value of prepared glasses increases with the increase of Y_2O_3. As a result of the creation of new links among YO_6 and the other structural units established in the glass matrices, this can accredit to the increasing network connectivity. Due to the formation of new linked B-O-Y bonds, the significant

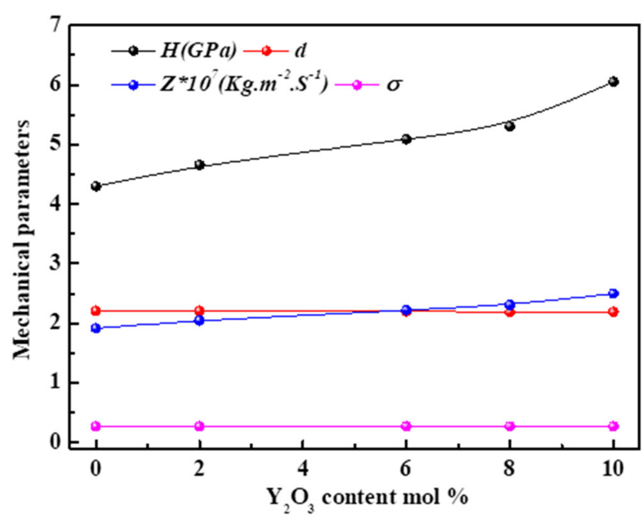

Fig. 9 Acoustic impedance (Z), dimensionality (*d*), Poisson ratio (σ) and micro-hardness (H) of glass system doped and undoped Y_2O_3 oxide by mol. %

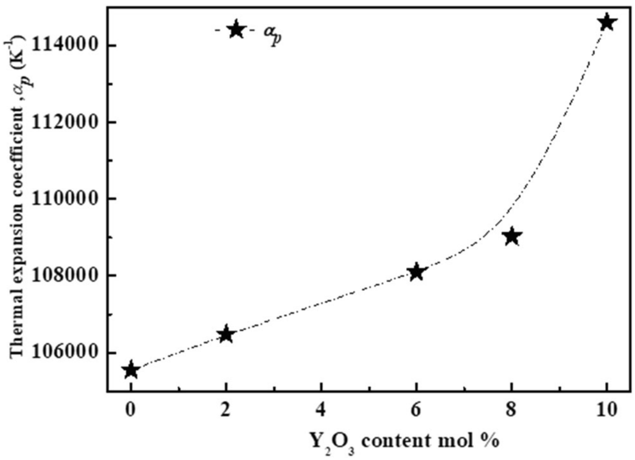

Fig. 10 Thermal expansion coefficient $\alpha_{P,}$ (K^{-1}), of glass system doped and undoped Y_2O_3 oxide by mol. %

increase in OPD, which is an indicator of the packing stiffness of the oxide network, suggests a packed amorphous structure. The increase in OPD with the addition of Y_2O_3 is also accredited to the creation of bridging oxygen (BO).

V_o value of prepared glasses decreases with the increase of Y_2O_3. V_o shows an inverse sequence with OPD. The reduction in $V_o$with the addition of Y_2O_3 may be accredited to the decrease in the V_m. The decreasing trend in V_o can be related to NBO disappearing and BO creation. OPD and $V_m$of prepared glasses exemplified in Fig. 3.

Table 3 Mass attenuation coefficients (in cm^2/g) in comparison with different glass samples

Samples	MAC, (MeV)	
	0.02	10
G5 [Present work]	58.8	0.0392
$20SiO_2$-$30Bi_2O_3$-$40B_2O_3$-$1Fe_2O_3$-$9Na_2O$	20.429	0.028
$66B_2O_3$-$5Al_2O_3$-$29Na_2O$	1.074	0.020
$5Bi_2O_3$-$61B_2O_3$-$5Al_2O_3$-$29Na_2O$	5.059	0.022
$10Bi_2O_3$-$56B_2O_3$- $5Al_2O_3$-$29Na_2O$	9.043	0.023
0PbO-$30SiO_2$–$46.67B_2O_3$–$23.33Na_2O$	1.386	0.023
5PbO-$25SiO_2$–$46.67B_2O_3$–$23.33Na_2O$	5.167	0.021
10PbO-$20SiO_2$–$46.67B_2O_3$–$23.33Na_2O$	8.952	0.024
$49.46SiO_2$–$26.38Na_2O$- 23.08CaO- $1.07P_2O_5$	3.982	0.024
$47.84SiO_2$–$26.67Na_2O$- 23.33CaO- $2.16P_2O_5$	3.985	0.023
$44.47SiO_2$–$27.26Na_2O$- 23.85CaO- $4.42P_2O_5$	4.057	0.024
$40.96SiO_2$–$27.87Na_2O$- 24.39CaO- $6.78P_2O_5$	4.113	0.024
$37.28SiO_2$–$28.52Na_2O$- 24.95CaO- $9.25P_2O_5$	4.061	0.024
$48.98SiO_2$–$26.67Na_2O$- 23.33CaO- $1.02P_2O_5$	3.983	0.023
$43.66SiO_2$–$28.12Na_2O$- 24.60CaO- $3.62P_2O_5$	4.100	0.024
$38.14SiO_2$–$29.62Na_2O$- 25.91CaO- $6.33P_2O_5$	4.190	0.022
$40.71SiO_2$–$28.91Na_2O$- 25.31CaO-5.07 P_2O_5	4.131	0.022

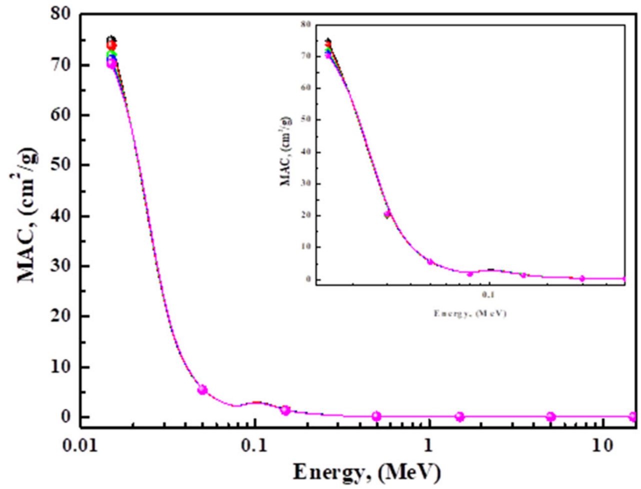

Fig. 11 Mass attenuation coefficient prepared glasses a function of photon energy according to Phy-X/PSD

Y^{+3} concentration computed $Y^{+3} = \left(\frac{6.023\times10^{23} x \ mol \ fraction \ of \ cation \times valency \ of \ cation}{Vm}\right)$. Because of molar volume reduction, it exemplified (Y^{+3}) enhanced. Quantified inter-ionic distance, $R_i = \left(\frac{1}{\text{Concentration of Y}}\right)^{\frac{1}{3}}$, the polaron radius r_p and internuclear distance r_i, determined as, $p = \frac{1}{2} \ \left(\frac{\pi}{6N}\right)^{\frac{1}{3}}, ri = \left(\frac{1}{N}\right)^{\frac{1}{3}}$. Y – Y separation (d_{Y-Y}) computed as $(dY-Y) = \left(\frac{V_m^B}{N}\right)^{\frac{1}{3}}$ and $V_m^B = \frac{Vm}{2(1-2Xn)}$. It has been confirmed that these perceived values reduce with Y, because of the reduction in molar volume. With the addition of Y_2O_3 content, these parameters decrease, which indicates that the network is more compact because of the creation (BO). This information is described in Table 2.

For BO or NBO connection confirmation, the coordinated average number is a significant criterion and characterized as $m = \sum n_{ci} X_i$ where cation coordination is n_{ci}. It was noticed

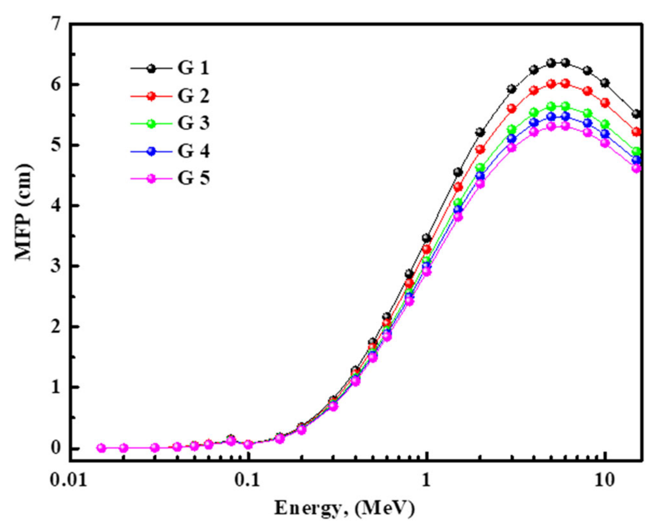

Fig. 12 Mean free path of prepared glasses a function of photon energy according to Phy-X/PSD

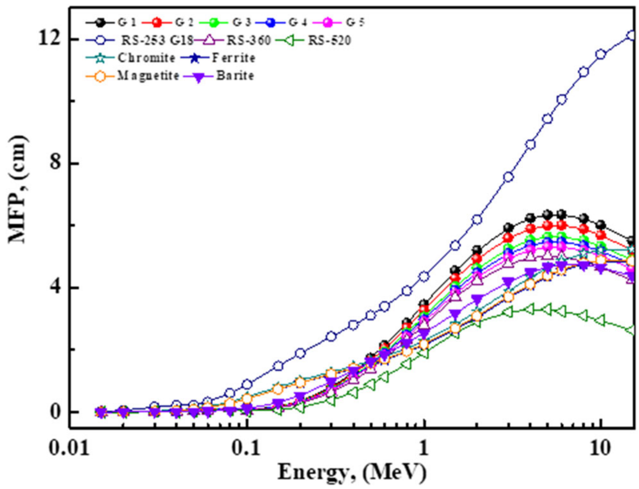

Fig. 13 Comparison of MFP of prepared glasses with other materials

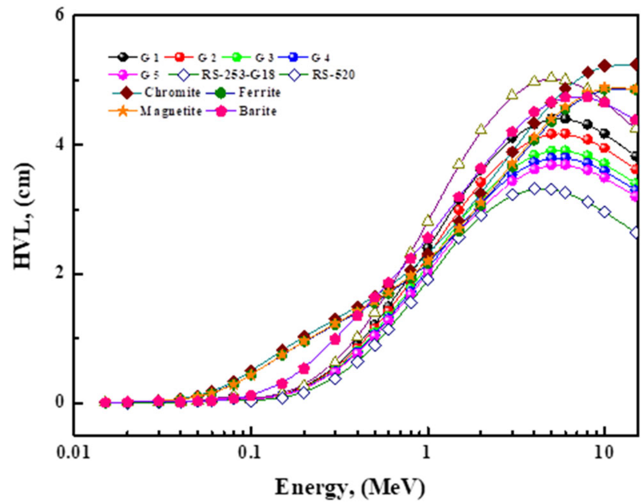

Fig. 15 Comparison of HVL of prepared glasses with other materials

that m increases with an increase in Y_2O_3 content. Calculate the number of bonds per unit as $n_b = \frac{N_A}{\ } V_m \sum n_{ci}X_i$. It discovered that perceived n_b through Y_2O_3 content increased.

The glass network influenced by the total number of mechanical constraints and computed as $N_{con} = N_{bs} + N_{bb}$ where N_{bb} is bond bending constraints and N_{bs} is bond stretching, $N_{bb} = \frac{\sum xi\ m}{2}$, $N_{bs} = \sum xi(2m-3)$. From the results of N_{con}, N_{bs} *and* N_{bb} we observed that, with an increment in Y_2O_3, the overall constraints of N_{con} are expected to enhance. Floppy modes considered as $M_f = 2 - \frac{5m}{6}$, cross-linking density D_{CL} considered as $D_{cl} = N_{con} - 2$, $CN_{eff} = \frac{2}{5} N_{con} + 3$. Results calculated to increase with increasing Y_2O_3 content. From the data of results obtained, it can be suggested that the glass ‘s enhance its 2D network with an increment in Y_2O_3.

3.3 Ultrasonic Studies

Figure 4 exemplified the ultrasonic velocities ($v_{L\&}v_T$) of the glass samples with Y_2O_3 content [25–33]. As exemplified in Fig. 4, the ultrasonic velocity of these samples enhanced by an increment in the Y_2O_3 concentration. Particularly, the increment in ultrasonic velocities was due to an increment in the network structure's connectivity. Thus, the transformation of the essential glass former B_2O_3 from BO_3 units to BO_4 units with increasing Y_2O_3 concentration explained the increase in both ultrasonic wave velocities in the investigated glass system. The structural groups of BO_4 are denser than BO_3 and are accountable for increment the binding of the glass structure and the compactness [25–33].

In this article, the elastic moduli behave in the same manner as observed for ultrasonic velocities as shown in Figs. 5 & 6. With the addition of Y_2O_3 content, the values of elastic moduli demonstrated a significant increase. The increment in

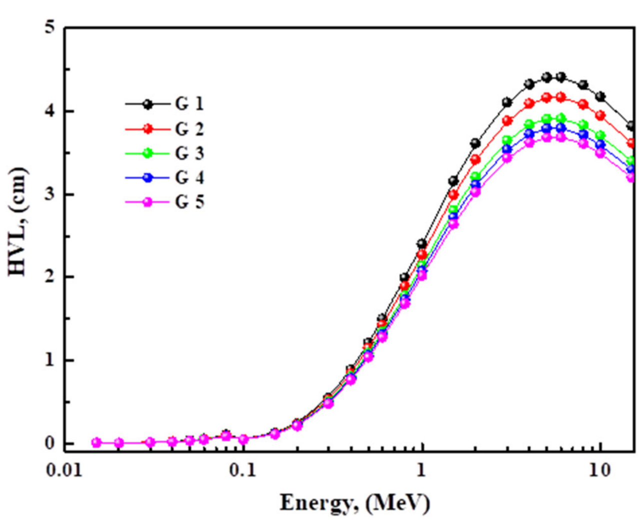

Fig. 14 Have value layer of prepared glasses a function of photon energy according to Phy-X/PSD

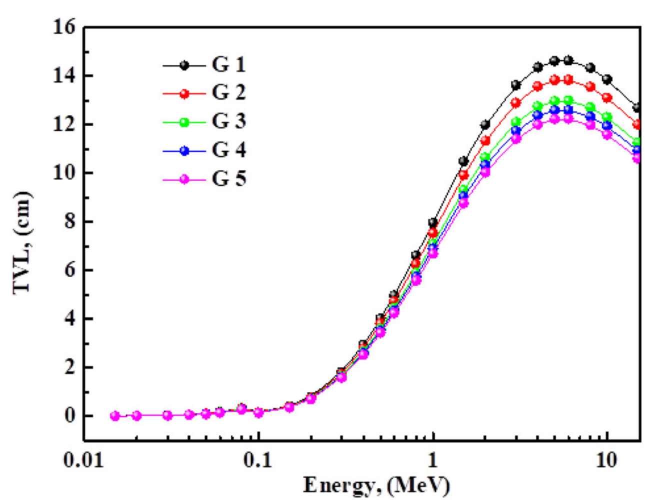

Fig. 16 Tenth value layer of prepared glasses a function of photon energy according to Phy-X/PSD

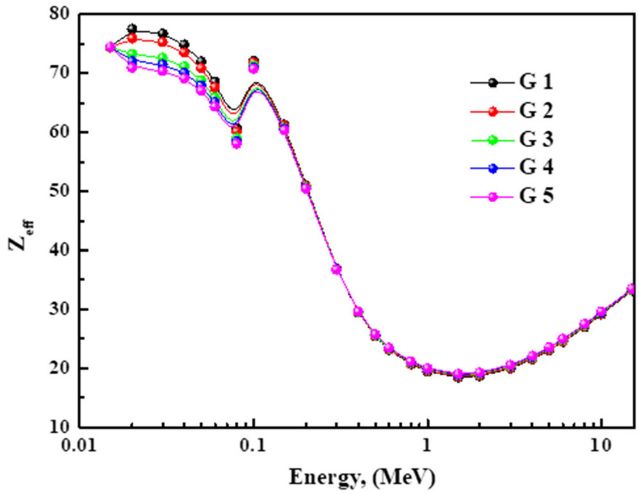

Fig. 17 Z_{eff} of prepared glasses a function of photon energy according to Phy-X/PSD

elastic modules with an increment in Y_2O_3 concentration was due to an increase in the number of coordinates and higher bond strength of YO_6 relative to BO_3 structural units.

A glass matrix's dimensionality (d) can attribute to the elastic moduli as $d = 4*(\frac{G}{K})$. For the examined glasses, the d values are about 2.2, i.e., the structure is a three-dimensional one with more cross-links that are increased. The Poisson ratio of these glasses demonstrated a constant value of about 0.27 ± 002. This value may have attributed to slight changes in the glass structure cross-link density. In identifying elastic moduli and atomic vibrations, the Debye temperature (θ_D) plays an important role. It considered that θ_D relies immediately on upon M_s. Thus, as Y_2O_3 content increases, θ_D and M_s increase as shown in Fig. 7. This have enhanced because of the conversion of BO_3 to YO_6, the expansion in cross-link density, and the structure of the glass connectivity. The values of V_i, G_i, H, Z, *and* α increased by the addition of Y_2O_3 as explained before. This information is described in Figs. 8, 9 & 10.

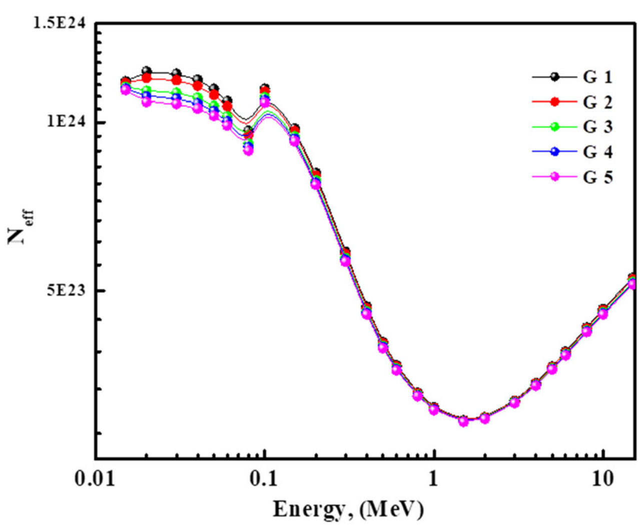

Fig. 18 N_{eff} of prepared glasses a function of photon energy according to Phy-X/PSD

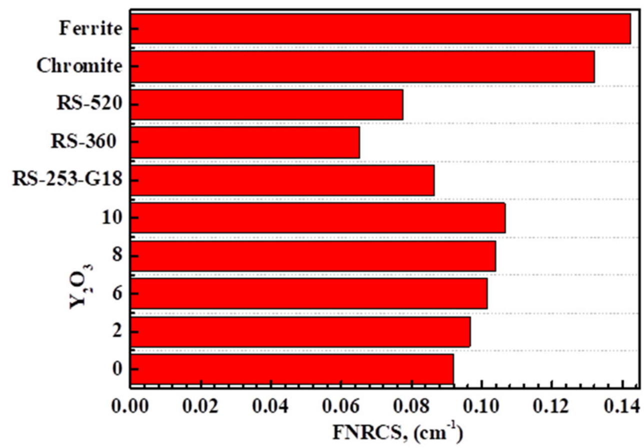

Fig. 19 FNRCS of prepared glasses a function of photon energy according to Phy-X/PSD

3.4 Photon Shielding Studies

By using Phy-X/PSD source code, the photon shielding competencies for the investigated glass under study have been introduced. For the glass system, essential features, such as MAC, LAC, MFP, TVL, and HVL, were quantified. The changes in MAC values with an energy range of 0.015–15 MeV are shown in Fig. 11. The highest values of MAC were found at low energy, and it has shift toward the greater energy, MAC decreased. The conduct of these concepts could attribute to the Photoelectric effect, Compton scattering, and pair production. On the other hand, due to the higher MAC value, we know that excellent photon shielding features can be achieved. Comparable improvement in MAC values with Y_2O_3 increased. In comparison to various glass samples, Table 3 shows coefficients of mass attenuation (in cm^2/g) [11, 34–39].

The average distance travelled by a movable photon collision was identified by MFP, so evaluating the MFP is very important. Figure 12 exemplified the MFP of the glass system against energy. It is obvious that with the increase of photon energy, the MFP values are increased. The MFP is ascending after certain photon energy, i.e., 0.1 meV. We can conclude that Y_2O_3 can establish MFP. Figure 13 exemplified the MFP of the glass system compared with other glasses.

Photon shielding materials are generally linked to create a more comprehension HVL. Figure 14 exemplified the HVL of the glass system against energy. It is obvious that with the increased photon energy, the HVL values are increasing. Figure 15 exemplified the HVL of the glass system compared with other glasses. It becomes more competitive with heavyweight concrete due to the decreasing HVL value in the RS-253 sample. We can summarize that the investigated glasses have a greater potential to contribute to use as radiation shielding materials. Figure 16 exemplified the TVL of the glass system against energy. It is obvious that with the increasing of photon energy, the TVL values are increased like HVL.

To determine the photon interactions of the glass system, Z_{eff} and N_{eff}'s values are calculated in this article. The findings of the Z_{eff} estimation linked to the radiation shielding function. Figures 15 & 16 exemplified Z_{eff} and N_{eff} of glass system against energy. As is visible in Figs. 17 & 18 glass with a higher Y_2O_3 value usually has higher Z_{eff}& N_{eff} values. Z_{eff} & N_{eff} values decrease in the energy range (0.01 < energy <1). In this selected region of energy, it can mention that Compton scattering is dominant. The highest Z_{eff} & N_{eff} values at the low-energy region and these alterations are insignificant. Z_{eff} & N_{eff} values reached to smallest value at the energy range (1 < energy <5). As is visible in Figs. 17 & 18 Compton effects, pair production, and photoelectric effects, where Z_{eff} & N_{eff} values are dominant.

Fast neutron removal cross-section (FNRCS) is shown in Fig. 19. It was noted that FNRCS increased with Y_2O_3. We can say that the addition of Y_2O_3 to glass samples enhances the FNRCS. Figure 19 exemplified FNRCS of glass system compared with other glasses as RS-253-G18, RS-360, RS-520, chromite, and ferrite. It becomes more competitive with RS-253-G18, RS-360, RS-520, due to its higher FNRCS values than the RS-253-G18, RS-360, and RS-520, samples, but it lower than values of the chromite and ferrite.

4 Conclusions

The melt-quenching method has been used to fabricate $52B_2O_3 - 12SiO_2–26Bi_2O_3 - (10-x)TiO_2$ - xY_2O_3, :$(0 \leq x \leq 10)$ glasses. The physical, mechanical, and shielding variables were examined for these glasses. The density of these samples increased while molar volume decreased. It was observed that ultrasonic velocities and elastic moduli (experimental and theoretical) for these glasses are increased. Gamma shielding characteristics of these glasses were predictable by the Phy-X / PSD program between 0.015–15 MeV. The effect of the addition of Y_2O_3 on the shielding ability of the glasses were discussed. Furthermore, it is possible to use present glass as a shield from radiation in the radio clinical building and x-ray centres.

Acknowledgments The authors would like to acknowledge the financial support of Taif University Researchers Supporting Project number (TURSP-2020/189), Taif University, Taif, Saudi Arabia.

Author Contributions **Kh. S. Shaaban** and **E. A. Abdel Wahab** performing, XRD, mechanical measurements and analysis, Writing-review, writing the manuscript, Methodology, Software, and writing – discussion. **K.H. Mahmoud, A.SA. Alsubaie,** and **Farid M. Abdel-Rahim,** Writing-review, writing the manuscript,

Data Availability My manuscript and associated personal data will be shared with Research Square for the delivery of the author dashboard.

Declarations The manuscript has not been published elsewhere and has not been submitted simultaneously for publication elsewhere.

Consent to Participate The authors consent to participate.

Consent for Publication The author's consent for publication.

Competing Interests The authors declare that they have no known competing financial interests or personal relationships that could have appeared to influence the work reported in this paper.

References

1. Shaaban KS, Abo-Naf SM, Hassouna MEM (2019) Physical and structural properties of Lithium borate glasses containing MoO_3. Silicon 11:2421–2428
2. El-Rehim AFA, Shaaban KS (2021) Influence of La_2O_3 content on the structural, mechanical, and radiation-shielding properties of sodium fluoro lead barium borate glasses. J Mater Sci Mater Electron 32:4651–4671
3. Shaaban KS, Abo-naf SM, Abd Elnaeim AM, Hassouna MEM (2017) Studying effect of MoO3 on elastic and crystallization behavior of lithium diborate glasses. Appl Phys A 123(6):457
4. Rao LS, Reddy MS, Rao DK, Veeraiah N (2009) Influence of redox behavior of copper ions on dielectric and spectroscopic properties of $Li_2O–MoO_3–B_2O_3$: CuO glass system. Solid-State Sciences 11(2):578–587
5. Abd-Allah WM, Saudi HA, Shaaban KS, Farroh HA (2019) Investigation of structural and radiation shielding properties of $40B_2O_3$–30PbO–(30-*x*) BaO-*x* ZnO glass system. Appl Phys A Mater Sci Process 125:275
6. Saudi HA, Abd-Allah WM, Shaaban KS (2020) Investigation of gamma and neutron shielding parameters for borosilicate glasses doped europium oxide for the immobilization of radioactive waste. J Mater Sci Mater Electron 31:6963–6976
7. Somaily HH, Shaaban KS, Makhlouf SA, Algarni H, Hegazy HH, Wahab EAA, Shaaban ER (2021) Comparative studies on Polarizability, optical basicity and optical properties of Lead borosilicate modified with Titania. J Inorg Organomet Polym 31:138–150
8. Wahab EAA, Shaaban KS (2018) Effects of SnO_2 on spectroscopic properties of borosilicate glasses before and after plasma treatment and its mechanical properties. Materials Research Express 5(2):025207
9. Koubisy MSI, Shaaban KS, Wahab EAA, Sayyed MI, Mahmoud KA (2021) Synthesis, structure, mechanical and radiation shielding features of $50SiO_2 - (48 + X) Na_2B_4O_7–(2 - X) MnO_2$ glasses. Eur Phys J Plus 136:156
10. Abdel Wahab EA, Koubisy MSI, Sayyed MI, Mahmoud KA, Zatsepin AF, Makhlouf SA, Shaaban KS (2021) Novel borosilicate glass system: $Na_2B_4O_7$-SiO_2-MnO_2 synthesis, average electronics polarizability, optical basicity, and gamma-ray shielding features. J Non-Cry Solids 553:120509
11. El-Rehim AFA, Zahran HY, Yahia IS et al. (2020). Physical, radiation shielding and crystallization properties of Na_2O-Bi_2O_3-

MoO_3-B_2O_3- SiO_2 Fe_2O_3 glasses. Silicon, https://doi.org/10.1007/s12633-020-00827-1

12. Shaaban KS, Yousef ES, Abdel Wahab EA, Shaaban ER, Mahmoud SA (2020) Investigation of crystallization and mechanical characteristics of glass and glass-ceramic with the compositions $x$$Fe_2O_3-35SiO_2-35B_2O_3-10Al_2O_3$-(20−$x$) Na_2O. J Materi Eng Perform 29:4549–4558
13. El-Rehim AFA, Zahran HY, Yahia IS et al (2021) Structural, elastic moduli, and radiation shielding of SiO2-TiO2-La2O3-Na2O glasses containing Y2O3. J Materi Eng Perform 30:1872–1884
14. Singh S, Kalia G, Singh K (2015) Effect of intermediate oxide (Y_2O_3) on thermal, structural and optical properties of Lithium borosilicate glasses. Mol Struct 1086:239–245
15. Shaaban KS, Wahab EAA, Shaaban ER, Yousef ES, Mahmoud SA (2020) Electronic Polarizability, optical basicity, thermal, mechanical and optical investigations of (65B_2O_3–30Li_2O–5Al_2O_3) glasses doped with Titanate. J of Elec Materi 49:2040–2049
16. Shaaban KS, Koubisy MSI, Zahran HY, Yahia IS (2020) Spectroscopic properties, electronic Polarizability, and optical basicity of titanium–cadmium Tellurite glasses doped with different amounts of lanthanum. J Inorg Organomet Polym 30:4999–5008
17. Shaaban KS, Wahab EAA, Shaaban ER, Yousef ES, Mahmoud SA (2020) Electronic polarizability, optical basicity and mechanical properties of aluminum lead phosphate glasses. Opt Quant Electron 52:125
18. Shaaban KS, Yousef ES, Mahmoud SA et al (2020) Mechanical, structural and crystallization properties in titanate doped phosphate glasses. J Inorg Organomet Polym 30:4655–4663
19. Şakar E, Özpolat ÖF, Alım B, Sayyed MI, Kurudirek M (2020) PhyX / PSD: development of a user friendly online software for calculation of parameters relevant to radiation shielding and dosimetry. Radiat Phys Chem 166:108496
20. Gedam RS, Ramteke DD (2012) Synthesis and characterization of Lithium borate glasses containing La2O3. Trans Indian Inst Metals 65:31–35
21. Shaaban KS, Yousef ES (2020) Optical properties of Bi2O3 doped boro tellurite glasses and glass ceramics. Optik – Inter J Light Ele Optics 203:163976
22. El-Rehim AFA, Shaaban KS, Zahran HY et al (2021) Structural and mechanical properties of Lithium bismuth borate glasses containing molybdenum (LBBM) together with their glass–ceramics. J Inorg Organomet Polym 31:1057–1065
23. Makishima A, Mackenzie JD (1973) Direct calculation of Young's modulus of glass. J Non-Cry Solids 12(1):35–45
24. Makishima A, Mackenzie JD (1975) Calculation of bulk modulus, shear modulus, and Poisson's ratio of glass. J Non-Cry solids 17(2): 147–157
25. Kodama M (1991) Ultrasonic velocity in sodium borate glasses. J Mater Sci 26:4048–4053
26. Veit U, Rüssel C (2017) Elastic properties of quaternary glasses in the MgO–CaO–Al_2O_3–SiO_2 system: modeling versus measurement. J Mater Sci 52:8159–8175
27. Shaaban KS, Saddeek YB, Sayed MA, Yahia IS (2018) Mechanical and thermal properties of Lead borate glasses containing CaO and NaF. Silicon 10:1973–1978
28. Shaaban KS, Ali AM, Saddeek YB, Aly KA, Dahshan A, Amin SA (2019) Synthesis, mechanical and optical features of Dy2O3 doped Lead alkali borosilicate glasses. Silicon 11:1853–1861
29. Shaaban KS, Saddeek YB, Sayed MA, Yahia IS (2017) Mechanical and thermal properties of Lead borate glasses containing CaO and NaF. Silicon 10:1973–1978
30. Shaaban KS, Saddeek YB (2017) Effect of MoO_3 content on structural, thermal, mechanical and optical properties of (B_2O_3-SiO_2-Bi_2O_3-Na_2O-Fe_2O_3) glass system. Silicon 9:785–793
31. El-Rehim AA, Zahran H, Yahia I et al (2020) Radiation, crystallization, and physical properties of cadmium borate glasses. Silicon. https://doi.org/10.1007/s12633-020-00798-3
32. Shaaban KS, Zahran HY, Yahia IS et al (2020) Mechanical and radiation-shielding properties of B2O3–P2O5–Li2O–MoO3 glasses. Appl Phys A 126(10):804
33. El-Rehim AFA, Ali AM, Zahran HY, Yahia IS, Shaaban KS (2021) Spectroscopic, structural, thermal, and mechanical properties of B_2O_3-CeO_2-PbO_2 glasses. J Inorg Organomet Polym 31:1774–1786
34. Mahmoud M, Makhlouf SA, Alshahrani B, Yakout HA, Shaaban KS, Wahab EAA (2021) Experimental and simulation investigations of mechanical properties and gamma radiation shielding of Lithium cadmium gadolinium silicate glasses doped erbium ions. Silicon. https://doi.org/10.1007/s12633-021-01062-y
35. El-Rehim A, AbdWahab F, Abdel EA, Halaka M, Abou M, Shaaban KS (2021) Optical properties of SiO2 – TiO2 – La2O3 – Na2O – Y2O3 glasses and a novel process of preparing the parent glass-ceramics. Silicon. https://doi.org/10.1007/s12633-021-01002-w
36. Alomairy S, Al-Buriahi M, Wahab EA, Sriwunkum C, Shaaban KS (2021) Synthesis, FTIR, and neutron/charged particle transmission properties of Pb3O4–SiO2–ZnO–WO3 glass system. Ceram Int. https://doi.org/10.1016/j.ceramint.2021.03.045
37. Fayad AM, Abd-Allah WM, Moustafa FA (2018) Effect of gamma irradiation on structural and optical investigations of borosilicate glass doped yttrium oxide. Silicon 10:799–809
38. Abdel Wahab EA, Shaaban KS, Elsaman R, Yousef ES (2019) Radiation shielding, and physical properties of lead borate glass doped ZrO_2 nanoparticles. Appl Phys A Mater Sci Process 125:869
39. El-Sharkawy RM, Shaaban KS, Elsaman R, Allam EA, El-Taher A, Mahmoud ME (2021) Investigation of mechanical and radiation shielding characteristics of novel glass systems with the composition xNiO-20ZnO-60B_2O_3-(20-x) CdO based on nano metal oxides. J Non-Cry Solids 528:119754